Effect of different electron donating groups on the performance of dye-sensitized solar cells

Haining Tian [a], Xichuan Yang [a,*], Jiayan Cong [a], Ruikui Chen [a], Chao Teng [a], Jing Liu [a], Yan Hao [a], Lei Wang [a], Licheng Sun [a,b,**]

[a] State Key Laboratory of Fine Chemicals, DUT-KTH Joint Education and Research Center on Molecular Devices, Dalian University of Technology (DUT), 158 Zhongshan Rd., 116012 Dalian, China
[b] School of Chemical Science and Engineering, Center of Molecular Devices, Organic Chemistry, Royal Institute of Technology(KTH), Teknikringen 30, 10044 Stockholm, Sweden

ARTICLE INFO

ABSTRACT

A series of organic sensitizers containing identical π-spacers and electron acceptors but different, aromatic amine electron-donating groups, were used in dye-sensitized solar cells to study the effect of the electron donating groups on device performance. The derived photophysical and photovoltaic properties, as well as density functional theory calculations, revealed that the tetrahydroquinoline dye was prone to aggregate upon the surface of titanium dioxide owing to the dye's planar structure. A 45% improvement in efficiency of a tetrahydroquinoline dye based cell was achieved when chenodeoxycholic acid was employed as co-adsorbent. However, the airscrew type of triphenylamine unit and Y type structure of the substituted phenothiazine framework suppressed dye aggregation on titanium dioxide. The efficiency of a phenothiazine dye-based cell fabricated using saturated co-adsorbent in dichloromethane was only 15% greater than that achieved in the absence of co-adsorbent. Electrochemical Impedance Spectroscopy was used to determine the interfacial charge transfer process occurring in solar cells that employed different dyes in both the absence and presence of chenodeoxycholic acid as co-adsorbent.

1. Introduction

Dye-sensitized solar cells (DSC's) have developed rapidly since Grätzel et al. first reported them in 1991 [1]. Many dyes have been used in DSC's, such as, coumarins [2,3], indolines [4–6], fluorines [7–9], triphenylamines [10–18], heteroanthracenes [19,20] and tetrahydroquinolines [21,22]. Generally, the dye consists of an electron-donating group (D), π-spacer (π) and electron acceptor (A). Small variations within these different sections cause significant differences in photovoltaic character. In earlier studies [10], the authors showed the effect of different π-spacers and electron acceptors on the performance of DSC's based on organic dyes. However, the electron-donating groups also play a crucial role in determining the solar energy-to-electricity conversion efficiency (η) of DSC. This paper concerns the effects of different aromatic amine electron-donating groups in three dyes (the phenothiazine

dye (**TH208**), triphenylamine dye (**D5**) [11] and tetrahydroquinoline dye (**C1-1**) [21]: Fig. 1) on photovoltaic performance.

2. Experimental

2.1. Analytical measurement

Absorption and emission spectra in solutions were recorded in a quartz cell with 1 cm path length on HP8453 (USA) and PTI700 (USA), respectively. ^{1}H NMR spectra were measured with varian INOVA 400 MHz (USA) with the chemical shifts against TMS. MS data were obtained with GCT CA156 (UK), HP1100 LC/MSD (USA) and LC/Q-TOF MS (UK). Electrochemical redox potentials were obtained by cyclic voltammetry (CV) using a three-electrode cell and an electrochemistry workstation (BAS100B, USA). The working electrode was a glass carbon electrode; the auxiliary electrode was a Pt wire and Ag/Ag^+ was used as reference electrode. Tetrabutylammonium hexaflourophosphate (TBAPF$_6$) 0.1 M was used as supporting electrolyte in CH_2Cl_2. Ferrocene was added to each sample solution at the end of the experiments and the ferrocenium/ferrocene (Fc/Fc$^+$) redox couple was used as an internal potential reference. The potentials versus NHE were calibrated by addition of

* Corresponding author. Tel.: +86 411 88993886; fax: +86 411 83702185.
** Corresponding author. Department of Chemistry, Organic Chemistry, Royal Institute of Technology (KTH), Teknikringen 30, 10044 Stockholm, Sweden. Tel.: +46 8 790 8127; fax: +46 8 791 2333.
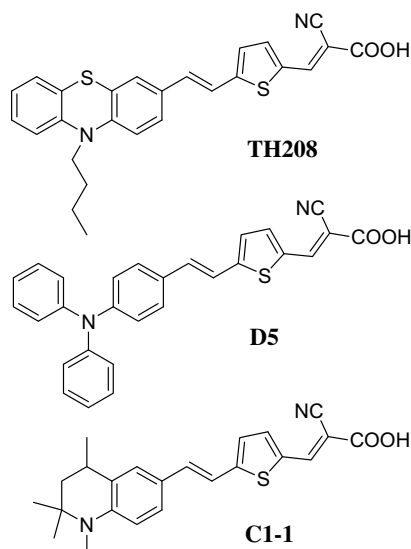E-mail addresses: yangxc@dlut.edu.cn (X. Yang), lichengs@kth.se (L. Sun).

Fig. 1. The structures of organic dyes **TH208**, **D5** and **C1-1**.

630 mV to the potentials versus Fc/Fc$^+$ [11]. Electrochemical impedance spectroscopy (EIS) for DSC under dark with bias −0.7 V was measured with an impedance/gain-phase analyzer (PARSTAT 2273, USA). The spectra were scanned in a frequency range of 10^{-2}–10^5 Hz at room temperature. The alternate current (AC) amplitude was set at 10 mV.

2.2. DSC fabrication

A layer of 13 nm paste (ca. 2 μm, T/SP, Solaronix, Switzerland) was coated on the F-doped tin oxide conducting glass (TEC15, 15Ω/ square, Pilkington, USA) by screen printing and then dried for 5 min at 125 °C. This procedure was repeated for 6 times (ca. 12 μm) and finally coated by a layer (ca. 4 μm) of titania paste (DHS-SLP1, Heptachroma, China) as scattering layer. The double-layer TiO$_2$ electrodes (area: 6 × 6 mm) were gradually heated under an air flow at 325 °C for 5 min, at 375 °C for 5 min, at 450 °C for 15 min, and at 500 °C for 15 min. The sintered film was further treated with 40 mM TiCl$_4$ aqueous solution at 70 °C for 30 min, then washed with ethanol and water, and annealed at 500 °C for 30 min. After the film was cooled to 40 °C, it was immersed into a 2×10^{-4} M dye bath (3×10^{-4} M for N719) and maintained under dark for 2 h (24 h for N719). The electrode was then rinsed with CH$_2$Cl$_2$ and dried. The hermetically sealed cells were fabricated by assembling the dye-loaded film as the working electrode and Pt-coated conducting glass as the counter electrode separated with a hot-melt Surlyn

1702 film (25 μm, Dupont). The electrolyte consisting of 0.6 M 1,2-dimethyl-3-propylimidazolium iodide (DMPII), 0.06 M LiI, 0.04 M I$_2$, and 0.4 M 4-*tert*-butylpyridine (TBP) in dry acetonitrile (MeCN) was introduced into the cell via vacuum backfilling by the hole in the back of the counter electrode. Finally, the hole was also sealed using Surlyn 1702 film and cover glass.

2.3. Photovoltaic properties measurement

The irradiation source for the photocurrent––voltage (*J*–*V*) measurement is an AM 1.5G solar simulator (16S-002, SolarLight Co. Ltd., USA). The incident light intensity was 100 mW cm^{-2} calibrated with a standard Si solar cell. The tested solar cells were masked to a working area of 0.159 cm^2. The current–voltage curves were obtained by linear sweep voltammetry (LSV) method using an electrochemical workstation (LK9805, Lanlike Co. Ltd., China). The measurement of the incident photon-to-current conversion efficiency (IPCE) was performed by a Hypermonolight (SM-25, Jasco Co. Ltd., Japan)

2.4. Synthesis of the dyes

D5 and **C1-1** dyes were synthesized according to our earlier publications [11,21], respectively. The synthesis route of **TH208** is shown in Fig. 2. The intermediate ***Bu*-PTZ-PPh$_3$·Br** was obtained according to our earlier publication [19].

2.4.1. Synthesis of ***Bu*-PTZ=T-CHO**

To a solution of 2, 5-dialdehyde thiophene (98 mg, 0.70 mmol), 18-crown-6 ether (10 mg) and anhydrous potassium carbonate (193 mg, 1.40 mmol) in 10 ml *N,N*-Dimethylformamide (DMF), another solution of ***Bu*-PTZ-PPh$_3$·Br** (500 mg, 0.73 mmol) in 10 ml DMF was added slowly with vigorously stirring at room temperature. The reaction was completed within 2 h. The reaction mixture was poured into water and extracted with dichloromethane (CH$_2$Cl$_2$, 10 ml × 3). The organic phase was collected and dried with anhydrous sodium sulfate. After removing the solvent, the residue was dissolved in 30 ml tetrahydrofuran (THF) to reflux in the presence of catalysis amount iodine for 8 h. The mixture was added diluted sodium hydroxide aqueous solution to remove iodine, then extracted with dichloromethane. Organic layer was dried with anhydrous sodium sulfate and removed the solvent. The residue was purified by column chromatography using silica gel and dichloromethane-petroleum ether (1/1; v/v) mixture as the eluent to give ***Bu*-PTZ=T-CHO** (*E*, red viscous liquid, 158 mg, yield 58%). ^{1}H NMR (Acetone-*d$_6$*, 400 MHz, ppm): δ 0.93 (3H, t), 1.45–1.51 (2H, m), 1.77–1.80 (2H, m), 3.97 (2H, t), 6.95 (1H, t), 7.04 (2H, dd, *J$_1$* = 2.2 Hz, *J$_2$* = 2.2 Hz), 7.14–7.23 (3H, m), 7.31 (1H, d, *J* = 4.0 Hz), 7.41 (1H, d, *J* = 16.2 Hz), 7.42–7.46 (2H, m), 7.86 (1H, d, *J* = 4.0 Hz), 9.89
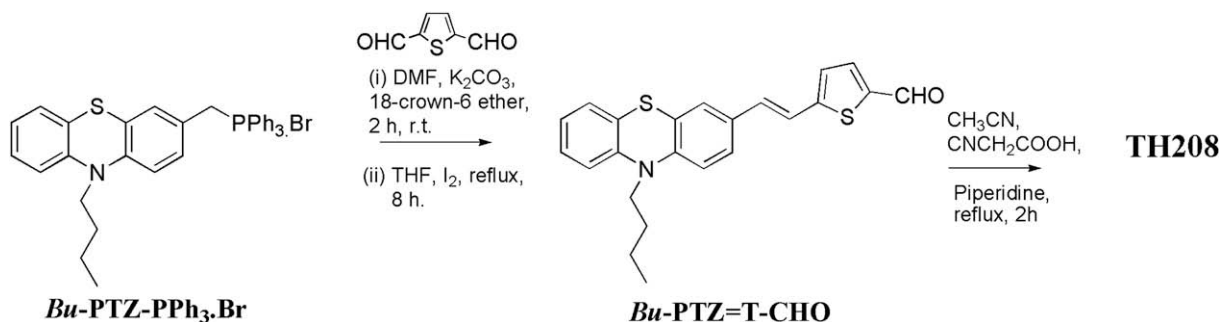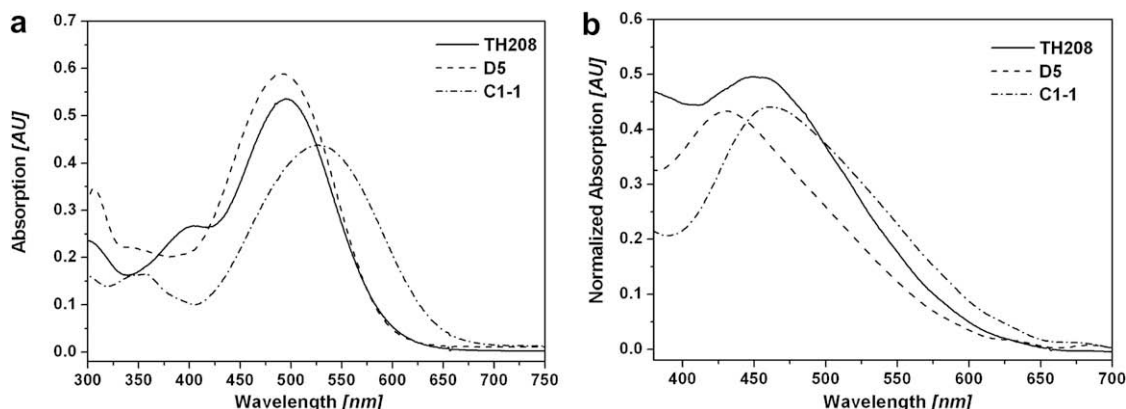

Fig. 2. The synthesis route of **TH208**.

Fig. 3. The absorption spectra of dyes in CH_2Cl_2 (a) and on TiO_2 film (b).

(1H, s). HR-MS ES$^+$ (m/z): calcd. for $C_{23}H_{21}NOS_2$, 391.1095; found, 391.1061.

2.4.2. Synthesis of TH208

An acetonitrile solution of **Bu-PTZ=T-CHO** (150 mg, 0.38 mmol) and cynaoacetic acid (85 mg, 1 mmol) was refluxed in the presence of piperidine for 2 h. After removing the solvent, the residue was purified by column chromatography using silica gel and dichloro-methane-methanol (10/1; v/v) mixed as the eluent to give product **TH208** (dark solid, 141 mg, 81%). ^{1}H NMR (Acetone-d_6, 400 MHz): δ 0.93 (3H, t), 1.46–1.51 (2H, m), 1.77–1.81 (2H, m), 3.99 (2H, t), 6.96 (1H, t), 7.05 (2H, d, $J = 8.2$ Hz), 7.15 (1H, d, $J = 7.7$ Hz), 7.21 (1H, m), 7.24 (1H, d, $J = 16.2$ Hz), 7.37 (1H, d, $J = 4.0$ Hz), 7.44 (1H, d, $J = 16.2$ Hz), 7.47–7.51 (2H, t), 7.89 (1H, d, $J = 4.0$ Hz), 8.41 (1H, s). HR-MS ES$^+$ (m/z): calcd. for $[C_{26}H_{22}N_2O_2S–CO_2]$, 414.1224; found, 414.1231.

3. Results and discussion

3.1. Photophysical properties

The absorption spectra of **TH208**, **D5** and **C1-1** dyes in CH_2Cl_2 and on TiO_2 films are shown in Fig. 3, and the corresponding data were collected in Table 1. In CH_2Cl_2 solution, **TH208**, **D5** showed the maximum absorption wavelength (λ_{abs}) 494 nm and 490 nm, respectively, which were corresponding to HOMO (highest occu-pied molecular orbital) → LUMO (lowest unoccupied molecular orbital) transition. Due to strong electron donating ability of tet-rahydroquinoline (THQ) unit, **C1-1** dye exhibited the λ_{abs} at 525 nm. The big π-conjugated systems mean that the three dyes are prone to form the aggregation. When **TH208**, **D5** and **C1-1** were sensitized on TiO_2 surface, the absorption maxima of these dyes were blue-shifted by 40, 60, and 65 nm in comparison to those in solution

respectively, due to H-aggregation on semiconductor surface [3]. The result suggested that the chenodeoxycholic acid (CDCA) as dye aggregation depressor should be added to dye-baths for following solar cell fabrication.

3.2. Electrochemical properties

To further study the possibilities of electron injection from the excited state dye to conduction band (CB) of semiconductor and the dye regeneration, the CV of these dyes were performed in CH_2Cl_2 to measure the redox potentials (see Fig. 4). The first oxidation potentials (E_{ox}) corresponding to the HOMO levels of the dyes were summarized in Table 1. The HOMO levels of **TH208**, **D5** and **C1-1** dyes are 0.88 V, 1.09 V and 0.77 V, respectively, which are positive enough comparing with that of iodine/iodide (0.4 V) [23], indi-cating that the oxidized dyes could be reduced effectively by elec-trolyte and then are regenerated. As we know, the HOMO level is mainly affected by electron donor. The electron donor with strong donating ability will shift the HOMO level more negative. Thus, from the HOMO level data of these dyes, we can conclude that the electron donating ability of these electron donors in the order THQ > PTZ > TPA. However, the reduced gap between ground state of dye and redox potential of electrolyte would lead to decreased regeneration efficiency of the oxidized dye by I$^-$, and thus result in the increasing of the dark current and the lower performances of the DSCs [21]. From the CV curves, we can find the three dyes are redox-stable, one-electron reversible at first oxidation potential. The first oxidation and reduction peaks can be observed clearly, suggesting that the first oxidized states of the dyes are stable [24].

The LUMO levels of these dyes can be obtained by HOMO level and zeroth–zeroth energy (E_{0-0}) of the dyes estimated from the intersection between the absorption and emission spectra, namely, HOMO–E_{0-0}. Molecular orbital energy diagram of HOMO and LUMO

Table 1
Absorption, emission, and electrochemical properties of **TH208**, **D5** and **C1-1**.

Dye	Absorption[a]			Emission	Oxidation potential[c]		
	λ_{abs} [nm]	ε at λ_{abs} [M^{-1} cm^{-1}]	λ_{abs} on TiO_2[b] [nm]	λ_{emi} [nm]	HOMO [V] (vs. NHE)	E_{0-0}[V][d] (Abs/Em)	LUMO [V] (vs.NHE)
TH208	494	27 000	454	704	0.88	2.15	−1.27
D5	490	29 000	430	676	1.09	2.12	−1.03
C1-1	525	22 000	460	712	0.77	1.96	−1.19

[a] Absorption, emission spectra were measured in CH_2Cl_2 solution at 25 °C (2×10^{-5} M).
[b] Absorption spectra on TiO2 were obtained through measuring the dye absorbed TiO_2 films in CH_2Cl_2.
[c] The oxidation potential of the dyes were measured in CH_2Cl_2 (working electrode: glassy carbon; reference electrode: Ag/Ag$^+$ counter electrode: Pt) with 0.1 M tetra-butylammonium hexafluorophosphate (TBAPF6) as electrolyte.
[d] E_{0-0} was estimated from the intersection between the absorption and emission spectra.
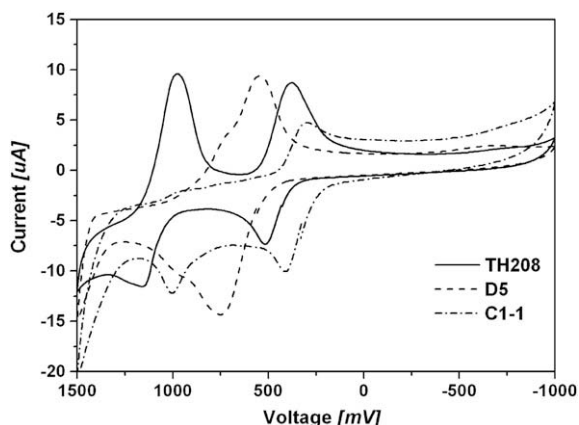
Fig. 4. The CV curves of dyes in CH_2Cl_2.

Table 2
The Photovoltaic data of DSC based on **TH208**, **D5** and **C1-1** dyes[a]

Dye	J_{SC} [mA cm^{-2}]	V_{OC} [V]	Fill factor [ff]	η [%]
TH208[b]	13.4	0.685	0.70	6.4
TH208[c]	12.2	0.638	0.72	5.6
D5[b]	12.4	0.665	0.73	6.0
D5[c]	10.7	0.615	0.73	4.8
C1-1[b]	14.5	0.651	0.68	6.4
C1-1[c]	10.4	0.583	0.72	4.4
N719[d]	16.9	0.699	0.68	8.0

[a] Irradiated light: AM 1.5 G (100 mW cm^{-2}); Working area: 0.159 cm^2; Electrolyte: 0.6 M 1,2-dimethyl-3-n-propylimidazolium iodide (DMPII)/0.06 M LiI/0.04 M I$_2$/0.4 MTBP in MeCN.
[b] Dye bath: CH_2Cl_2 solution (2×10^{-4} M) with saturated CDCA, 2 h.
[c] Dye bath: CH_2Cl_2 solution (2×10^{-4} M), 2 h.
[d] Dye bath: ethanol solution (3×10^{-4} M).

of dyes are shown in Fig. 5. To effectively inject the electron into the CB of TiO$_2$, the LUMO levels of the dyes must be sufficiently more negative than the conducing band energy (E_{cb}) of semiconductor, −0.5 V (*vs.* NHE) [23]. From the LUMO values, we can find all of the dyes can achieve the electron injection and form the oxidized dyes. The relatively large energy gaps between the LUMO of the dye and E_{cb} of semiconductor are sufficient for efficient electron injection, and also allow for the treatment the 4-*tert*-butylpyridine (TBP) to the electrolyte, which shift the E_{cb} of the TiO$_2$ negatively and improve the open-circuit voltage and total conversion efficiency consequently [25].

3.3. Photovoltaic properties

The photovoltaic properties of the solar cells fabricated with these organic dyes were measured under simulated AM 1.5G irradiation (100 mW cm^{-2}). To investigate the effect of CDCA on DSC performance, all the cells were fabricated in CH$_2$Cl$_2$ with saturated CDCA and without CDCA for comparison. We have not optimized the concentration of the co-adsorbent because the CDCA has very low solubility in CH$_2$Cl$_2$. So we just employed the saturated CDCA as co-adsorbent. The open-circuit photovoltage (Voc), short-circuit photocurrent density (Jsc), fill factor (ff), and solar energy-to-electricity conversion efficiencies (η) were listed in Table 2. Photocurrent density–voltage (J–V) characteristics and

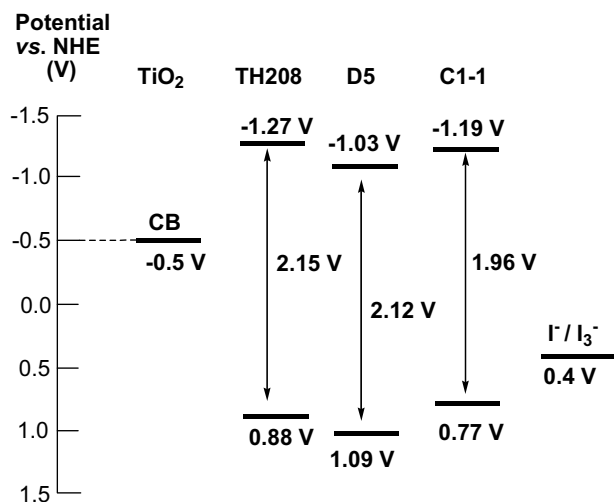incident photon-to-current conversion efficiencies (IPCEs) of devices based on these dyes are shown in Figs. 6 and 7, respectively. The sensitization conditions of these organic dyes were determined to be 2×10^{-4} M in CH$_2$Cl$_2$ with/without CDCA for 2 h, and the electrolytes is 0.6 M DMPII/0.06 M LiI/0.04 M I$_2$/0.4 MTBP in dried acetonitrile. Depending on the different electron donating groups, these dyes showed distinguishing and interesting results. All the η and IPCE values of DSC based on **TH208**, **D5** and **C1-1** dyes have been improved by the addition of CDCA (see Figs. 6 and 7), indicating the dyes indeed aggregate on TiO$_2$ films. There is 45% improvement in η value of DSC based on **C1-1** when the CDCA is added to dye-bath due to suppressing the serious aggregation effectively. From Fig. 8, we found the IPCE values of **C1-1** based DSC with CDCA as coadsorbent showed significant improvement, resulting in the higher J_{SC} (14.5 mA cm^{-2}) than that without CDCA (10.4 mA cm^{-2}). However, the DSC based on **TH208** fabricated in CH$_2$Cl$_2$ with saturated CDCA only obtained 15% improvement compared with that without CDCA as coadsorbent. Under the optimized test condition, the DSC based **TH208**, **D5** and **C1-1** dyes obtained the η values 6.4% (J_{SC} = 13.4 mA cm^{-2}, V_{OC} = 0.685 V, ff = 0.70), 6.0% (J_{SC} = 12.4 mA cm^{-2}, V_{OC} = 0.665 V, ff = 0.73) and 6.4% (J_{SC} = 14.5 mA cm^{-2}, V_{OC} = 0.651 V, ff = 0.68) respectively. **D5** based DSC exhibited narrow IPCE spectrum (300 ∼ 660 nm), but with the highest values between 440 nm and 520 nm. **C1-1** based DSC showed the broadest IPCE spectrum (300 ∼ 760 nm) with exceeding 80% values from 440 nm to 600 nm. Under similar test condition, a device based on referenced N719 dye showed 8.0% efficiency (J_{SC} = 16.9 mA cm^{-2}, V_{OC} = 0.699 V, ff = 0.68).

Fig. 5. Molecular orbital energy diagram of HOMO and LUMO of dyes.

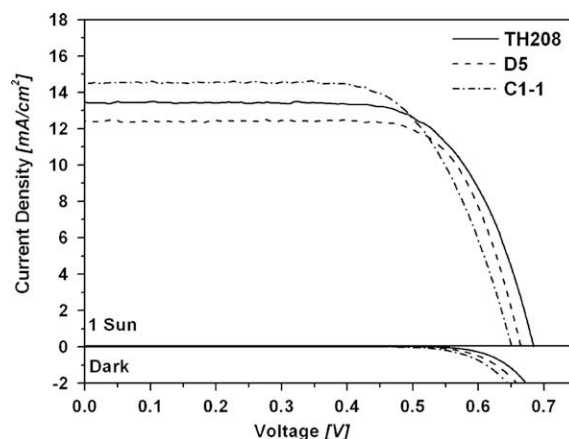**Fig. 6.** The J–V curves of DSC based on **TH208**, **D5** and **C1-1** dye with CDCA.

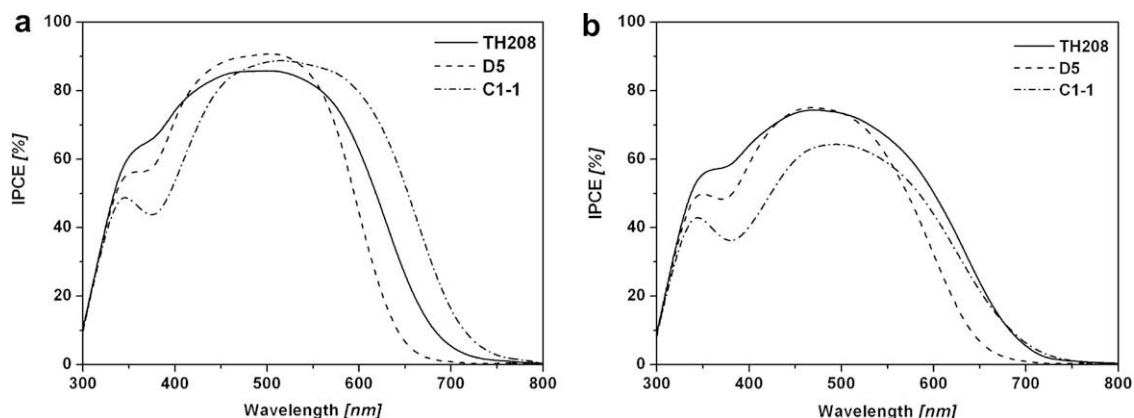**Fig. 7.** The IPCE spectra of DSC fabricated in CH_2Cl_2 with saturated CDCA (a) and without CDCA (b).

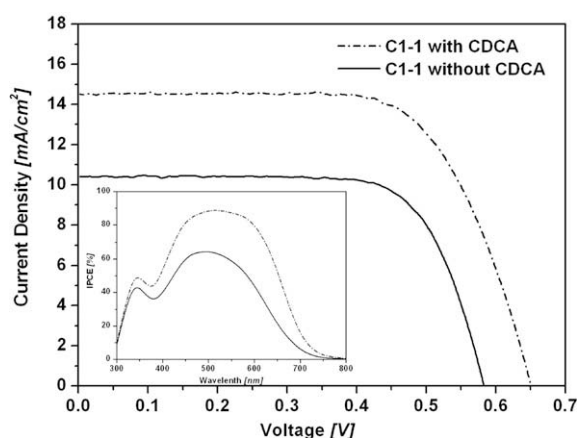**Fig. 8.** The *J-V* curves and IPCE spectra (insert) of **C1-1** based DSC fabricated in CH_2Cl_2 with saturated CDCA and without CDCA.

3.4. Electrochemical impedance spectroscopy

Electrochemical impedance spectroscopy (EIS) analysis [26–29] was performed to study the interfacial charge transfer processes in DSC based on different dyes. The selected Nyquist plot and Bode phase plot are shown in Fig. 9. The Nyquist plots (Fig. 9a) showed the radius of the middle semicircle to increase in the order **D5**<**TH208** < **C1-1** with CDCA, indicating that electron recombination augments from **D5** to **C1-1**. The electron lifetimes obtained by fitting the curves are 34.4, 32.8 and 41.3 ms, respectively. The longer electron lifetime indicates the effective suppression of back reaction between the electrons in TiO_2 and redox electrolyte, and means the improvement of photocurrent and photovoltage [29]. However, there are few differences in photovoltages of DSC based on these dyes with CDCA. Therefore, the longer lifetime will result in the higher photocurrent. When the DSC were fabricated with these dyes and CDCA was not employed to act as the coabsorbent, the electron lifetimes of **TH208**, **D5** and **C1-1** based DSC became shorter and there are only 14.0, 13.7 and 7.4 ms, respectively. From the Bode plots (Fig. 9b), the high-frequency peaks correspond to charge transfer at the counter electrode. There was no significant change in the position of the high-frequency peaks for the three dyes studied. The middle frequency peak of DSC based **C1-1** with CDCA shifted to lower frequency relative to the **C1-1** device without CDCA, indicating a longer lifetime for the former species. We considered the addition of CDCA will cause the dyes forming compact and monomolecular adsorption on TiO_2 surface due to the bulky CDCA molecule, and thus suppressed the back reaction, especially for **C1-1** dye. Without CDCA addition, the H-aggregation will perform the negative effect on the electron injection and also cannot decrease the back reaction effectively, resulting in the lower photocurrent and photovoltage. The result is agreement with the photovoltaic data.

3.5. Molecular orbital calculations

To get a further insight into the big difference in performance of DSC based on these dyes, density functional theory (DFT) calculations [30] were performed at a B3LYP/6–31 + g(d) level for the geometry optimization. The optimized structures and electron distribution of the HOMO and LUMO of these dyes were shown in
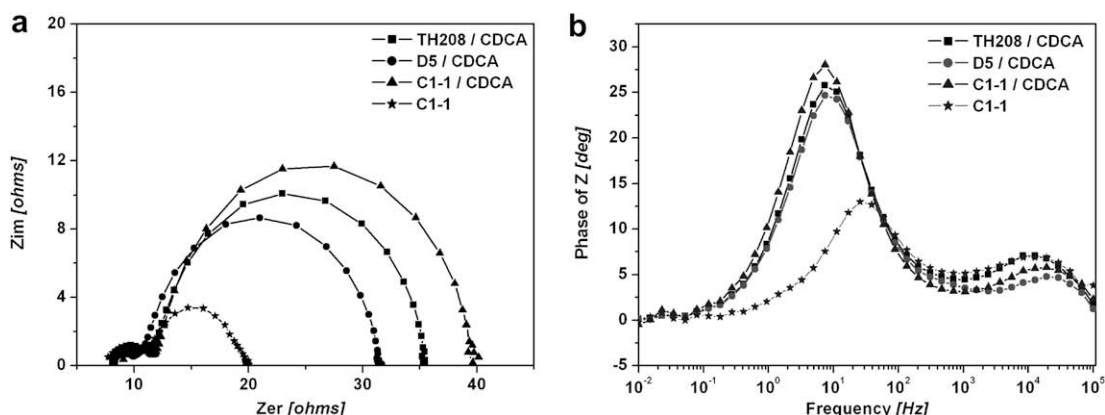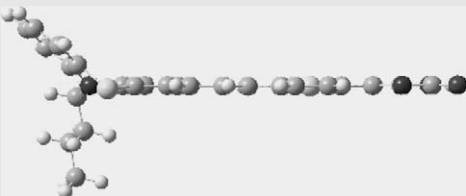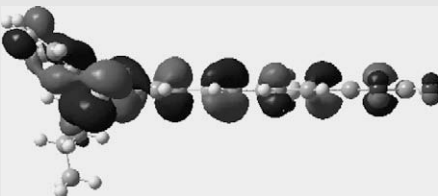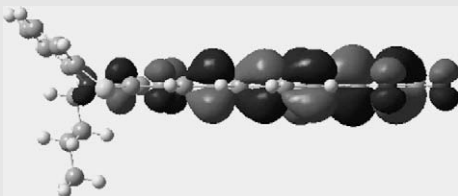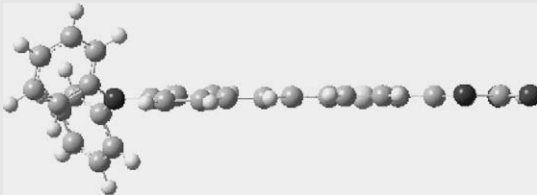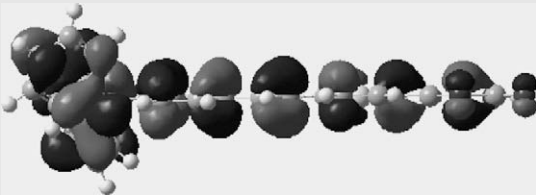

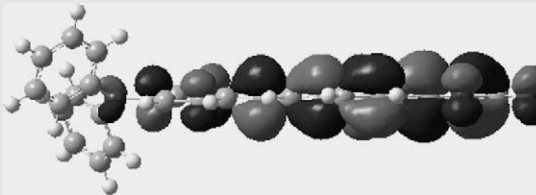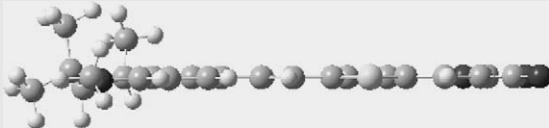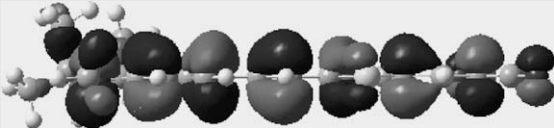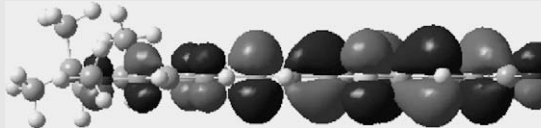**Fig. 9.** EIS spectra for the DSC made with different dyes a: Nyquist plots; b: Bode phase plots.

Table 3
The optimized structure and HOMO and LUMO electron distributions of **TH208**, **D5** and **C1-1** dyes[a]

Dye	Optimized structure	HOMO	LUMO
TH208			
D5			
C1-1			

[a] Density functional theory (DFT) calculations were performed at a B3LYP/6-31 + g(d) level for the geometry optimization.

Table 3. According to the optimized dye structures, **C1-1** with coplanar molecular structure is prone to form the serious H-aggregation on TiO₂. The electron donor section of **D5** exhibits airscrew form and the substituted PTZ framework of **TH208** is a Y type structure. The HOMO is mainly located on the electron donating group and π-spacer, and the LUMO is located in electron withdrawing groups through the π-spacer. It reveals that the thiophene π-spacer is essentially coplanar with cyanoacrylic acid group. There are effective electron separations between HOMO and LUMO of these dyes induced by light irradiation.

4. Conclusion

To further study the effect of different electron donating groups of organic sensitizers on DSC performance, a novel phenothiazine dye (**TH208**) was designed and synthesized to compare with **D5** and **C1-1** dyes reported in earlier literature. Different electron donating groups of organic sensitizers show different interaction on TiO₂ surface. The coplanar structure of **C1-1** displays serious H-aggregation on TiO₂ films. There is 45% improvement in η value of DSC based on **C1-1** when the CDCA is added to dye-bath. According to the data, the addition of CDCA can improve the η values. However, the CDCA probably occupy the effective adsorption position on TiO₂ surface and decreases the adsorbed amount of sensitizers on TiO₂ surface. Non-planar structures of **TH208** and **D5** could suppress the aggregation more or less. The DSC based on **TH208** fabricated in CH₂Cl₂ with saturated CDCA only obtains 15% improvement compared with that without CDCA as coadsorbent due to the weak aggregation. The result suggests that the non-planar structures of organic sensitizers could be further designed to complete the monomolecular adsorption without suppressor and obtain the more prominent performance of DSC.

References

[1] O'Regan B, Grätzel M. A low-cost, high-efficiency solar cell based on dye-sensitized colloidal TiO₂ films. Nature 1991;353:737–40.

[2] Hara K, Sayama K, Ohga Y, Shinpo A, Suga S, Arakawa H. A coumarin-derivative dye sensitized nanocrystalline TiO₂ solar cell having a high solar-energy conversion efficiency up to 5.6%. Chemical Communications 2001;6:569–70.

[3] Hara K, Wang Z, Sato T, Furube A, Katoh R, Sugihara H, et al. Oligothiophene-containing coumarin dyes for efficient dye-sensitized solar cells. Journal of Physical Chemistry B 2005;109(32):15476–82.

[4] Horiuchi T, Miura H, Sumioka K, Uchida S. High efficiency of dye-sensitized solar cells based on metal-free indoline dyes. Journal of the American Chemical Society 2004;126(39):12218–9.

[5] Ito S, Miura H, Uchida S, Takata M, Sumioka K, Liska P, et al. High-conversion-efficiency organic dye-sensitized solar cells with a novel indoline dye. Chemical Communications 2008;41:5194–6.

[6] Liu B, Zhu W, Zhang Q, Wu W, Xu M, Ning Z, et al. Conveniently synthesized isophorone dyes for high efficiency dye-sensitized solar cells: tuning photovoltaic performance by structural modification of donor group in donor-π-acceptor system. Chemical Communications 2009;13:1766–8.

[7] Kim S, Lee J, Kang S, Ko J, Yum J, Fantacci S, et al. Molecular engineering of organic sensitizers for solar cell applications. Journal of the American Chemical Society 2006;128(51):16701–7.

[8] Choi H, Baik C, Kang S, Ko J, Kang M, Nazeeruddin Md K, et al. Highly efficient and thermally stable organic sensitizers for solvent-free dye-sensitized solar cells. Angewandte Chemie, International Edition 2008;47(2):327–30.

[9] Qin H, Wenger S, Xu M, Gao F, Jing X, Wang P, et al. An organic sensitizer with a fused dithienothiophene unit for efficient and stable dye-sensitized solar cells. Journal of the American Chemical Society 2008;130(29):9202–3.

[10] Tian H, Yang X, Chen R, Zhang R, Hagfeldt A, Sun L. Effect of different dye baths and dye-structures on the performance of dye-sensitized solar cells based on triphenylamine dyes. Journal of Physical Chemistry C 2008;112(29):11023–33.

[11] Hagberg D, Edvinsson T, Marinado T, Boschloo G, Hagfeldt A, Sun L. A novel organic chromophore for dye-sensitized nanostructured solar cells. Chemical Communications 2006;21:2245–7.

[12] Hagberg D, Yum J, Lee H, Angelis F, Marinado T, Karlsson K, et al. Molecular engineering of organic sensitizers for dye-sensitized solar cell applications. Journal of the American Chemical Society 2008;130(19):6259–66.

[13] Velusamy M, Thomas K, Lin J, Hsu Y, Ho K. Organic dyes incorporating low-band-gap chromophores for dye-sensitized solar cells. Organic Letters 2005;7(10):1899–902.

[14] Kitamura T, Ikeda M, Shigaki K, Inoue T, Anderson N, Ai X, et al. Phenyl-conjugated oligoene sensitizers for TiO₂ solar cells. Chemistry of Materials 2004;16(9):1806–12.

[15] Li G, Jiang K, Li Y, Li S, Yang L. Efficient structural modification of triphenyl-amine-based organic dyes for dye-sensitized solar cells. Journal of Physical Chemistry C 2008;112(30):11591–9.

[16] Ning Z, Zhang Q, Wu W, Pei H, Liu B, Tian H. Starburst triarylamine based dyes for efficient dye-sensitized solar cells. Journal of Organic Chemistry 2008; 73(10):3791–7.

[17] Zhang G, Bala H, Cheng Y, Shi D, Lv X, Yu Q, et al. High efficiency and stable dye-sensitized solar cells with an organic chromophore featuring a binary π-conjugated spacer. Chemical Communications 2009;16:2198–200.

[18] Li G, Zhou Y, Cao X, Bao P, Jiang K, Lin Y, et al. Novel TPD-based organic D–π–A dyes for dye-sensitized solar cells. Chemical Communications 2009;16: 2201–3.

[19] Tian H, Yang X, Chen R, Pan Y, Li L, Hagfeldt A, et al. Phenothiazine derivatives for efficient organic dye-sensitized solar cells. Chemical Communications 2007;36:3741–3.

[20] Tian H, Yang X, Chen R, Hagfeldt A, Sun L. A metal-free "black-dye" for panchromatic dye-sensitized solar cells. Energy & Environmental Science 2009;2:674–7.

[21] Chen R, Yang X, Tian H, Wang X, Hagfeldt A, Sun L. Effect of tetrahy-droquinoline dyes structure on the performance of organic dye-sensitized solar cells. Chemistry of Materials 2007;19(16):4007–15.

[22] Chen R, Yang X, Tian H, Sun L. Tetrahydroquinoline dyes with different spacers for organic dye-sensitized solar cells. Journal of Photochemistry and Photobiology, A: Chemistry 2007;189(2-3):295–300.

[23] Hagfeldt A, Grätzel M. Light-induced redox reactions in nanocrystalline systems. Chemical Reviews 1995;95(1):49–68.

[24] Ooyama Y, Ishii A, Kagawa Y, Imae I, Harima Y. Dye-sensitized solar cells based on novel donor-acceptor π-conjugated benzofuro[2,3-c]oxazolo[4,5-a]carbazole-type fluorescent dyes exhibiting solid-state fluorescence. New Journal of Chemistry 2007;31(12):2076–82.

[25] Boschloo G, Häggman L, Hagfeldt A. Quantification of the effect of 4-tert-butylpyridine addition to I-/I3- redox electrolytes in dye-sensitized nano-structured TiO2 solar cells. Journal of Physical Chemistry B 2006;110(26): 13144–50.

[26] Adachi M, Sakamoto M, Jiu J, Ogata Y, Isoda S. Determination of parameters of electron transport in dye-sensitized solar cells using electrochemical impedance spectroscopy. Journal of Physical Chemistry B 2006;110(28):13872–80.

[27] Wang Q, Moser J, Grätzel M. Electrochemical impedance spectroscopic analysis of dye-sensitized solar cells. The Journal of Physical Chemistry B 2005;109(31):14945–53.

[28] Wang Z, Koumura N, Cui Y, Takahashi M, Sekiguchi H, Mori A, et al. Hex-ylthiophene-functionalized carbazole dyes for efficient molecular photovoltaics: tuning of solar-cell performance by structural modification. Chemistry of Materials 2008;20(12):3993–4003.

[29] Kuang D, Uchida S, Humphry-Baker R, Zakeeruddin S, Grätzel M. Organic dye-sensitized ionic liquid based solar cells: remarkable enhancement in performance through molecular design of indoline sensitizers. Angewandte Chemie, International Edition 2008;47(10):1923–7.

[30] Frisch M, Trucks G, Schlegel H, Scuseria G, Robb M, Cheeseman J, et al. Gaussian 03, revision C.02. Wallingford, CT: Gaussian, Inc.; 2004.